

Cite this: *Inorg. Chem. Front.*, 2020, 7, 2637

Slow magnetic relaxation in hexacoordinated cobalt(II) field-induced single-ion magnets†

Anna Świtlicka,^a Barbara Machura,^a Mateusz Penkala,^b Alina Bieńko,^{b,c} Dariusz C. Bieńko,^d Ján Titiš,^e Cyril Rajnák,^e Roman Boča^e and Andrew Ozarowski^f

To gain a better insight into the factors affecting the enhancement of the energy barrier in single molecule (single ion) magnets, three hexacoordinate cobalt(II) complexes based on the tridentate ligand 2,6-bis(pyrazol-1-yl)pyridine (pypz) and pseudohalide ions have been synthesized and investigated. It was found that dicyanoamido and azido ligands act as bridges to form a one dimensional network based on a single $\mu_{1,5}$ -dca bridge [Co(pypz)(dca)(H₂O)]₂·dca (**1**) and dimer [Co₂(pypz)₂($\mu_{1,1}$ -N₃)₂(N₃)₂·2CH₃OH] (**2**), while tcm[−] counterbalanced the charge of [Co(pypz)₂]²⁺ in [Co(pypz)₂](tcm)₂ (**3**), where dca[−] = dicyanamide ion; tcm[−] = tricyanomethanide ion, respectively. The DC magnetic data show a sizable magnetic anisotropy, which was confirmed by high-field/high frequency EPR measurements. Two of them are SIMs (**1** and **3**) and the other one is a SMM (**2**). All complexes exhibit field induced slow magnetic relaxation with two (**1** and **2**) or three relaxation channels (**3**) and an exceptionally long relaxation time for the low-frequency channel upon application of an external field $B_{DC} = 0.4, 0.3, \text{ and } 0.4 \text{ T}$ at $T = 1.9 \text{ K}$; $\tau(LF) = 1.9, 2.1 \text{ and } 0.9 \text{ s}$, respectively. Additionally, the high spin-reversal barriers, $U = 103 \text{ K}$ for **1** and 95 K for **2**, are among the largest for field-induced SIMs for cobalt(II) reported in the literature.

Received 27th February 2020,
Accepted 21st May 2020

DOI: 10.1039/d0qi00257g

rs.c.li/frontiers-inorganic

Introduction

Single-molecule magnetism (SMM) has attracted a lot of research interest since its first identification in 1993 by Gatteschi and co-workers in a dodecametallic manganese-acetate cage (Mn₁₂Ac).¹ To a large extent, the studies in this field have been driven by the wide application potential of SMM compounds that exhibit slow magnetic relaxation upon removal of a magnetizing field and magnetic hysteresis below

the blocking temperature. Such applications may include denser data storage and quantum computing.^{2–9} The SMM field has expanded to single-ion magnets (SIMs) and single-chain magnets (SCMs). Subsequently, magnetic anisotropy and relaxation dynamics were reported for mononuclear lanthanide-based and then for transition metal complexes,^{10–18} as well as one-dimensional polymeric (1D) transition metal compounds.^{19–25} The construction of these unconventional materials is based on the unique combination of high spin and magnetic anisotropy resulting in a magnetically bistable molecule with a high barrier for thermally activated relaxation of magnetization. Therefore, many examples, especially SIMs assembled from the anisotropic Co(II) ion, have appeared in the literature.^{26–29}

Contrary to traditional SMMs, whose axial zero-field splitting (ZFS) parameter is certainly negative, the sign and magnitude of magnetic anisotropy in Co-based SIMs depend on more varied and complex parameters.³⁰ In the range of mononuclear penta- or hexa-coordinated Co(II) complexes, strong magnetic anisotropies with both a negative ZFS parameter D and an easy-plane anisotropy ($D > 0$) can be obtained, and field-induced slow magnetic relaxation can be observed regardless of the sign of the D values.³¹

Special attention has been paid to establishing a magneto-structural correlation based on D for mononuclear hexa-coordinated d^7 compounds, especially Co(II) SIMs with large

^aDepartment of Crystallography, Institute of Chemistry, University of Silesia, 9 Szkolna St., 40-006 Katowice, Poland. E-mail: anna.switlicka@us.edu.pl

^bDepartment of Inorganic, Organometallic Chemistry and Catalysis, Institute of Chemistry, University of Silesia, 9 Szkolna St., 40-006 Katowice, Poland

^cFaculty of Chemistry, University of Wrocław, 14 F. Joliot-Curie, 50-383 Wrocław, Poland. E-mail: alina.bienko@chem.uni.wroc.pl

^dFaculty of Chemistry, Wrocław University of Technology, Wybrzeże Wyspiańskiego 27, 50-370 Wrocław, Poland

^eDepartment of Chemistry, Faculty of Natural Sciences, University of SS Cyril and Methodius, 917 01 Trnava, Slovakia

^fNational High Magnetic Field Laboratory, Florida State University, 1800 East Paul Dirac Drive, Tallahassee, Florida 32310, USA

† Electronic supplementary information (ESI) available: Syntheses, analytical and X-ray structural data, AC susceptibility data. Experimental section, XRPD spectra, crystal data and structure refinement and bond lengths [Å] and angles, AC susceptibility, field vs. frequency map of the resonances for **1–3**. CCDC 1973544–1973546. For ESI and crystallographic data in CIF or other electronic format see DOI: 10.1039/d0qi00257g

positive or negative D values.³² Even though a remarkable number of Co(II)-based SIMs have been reported so far, their effective energy barriers for spin reversal usually range from 20 to 50 K. For this reason, great efforts have been made towards finding a solid conceptual explanation for this behaviour. However, the parameters governing magnetic anisotropy are still poorly understood and the daunting task of having precise control over the magnetic anisotropy remains a difficult challenge.

In principle, the magnetic anisotropy and relaxation dynamics of mononuclear complexes can be fine-tuned by controlling the ligand field strength and symmetry of the crystal field. Along this line the present research concerns the preparation, structural characterization and variable-temperature magnetic and EPR studies of cobalt(II) complexes with 2,6-bis(pyrazol-1-yl)pyridine (pypz) and dca^- , N_3^- , tcm^- anions. The Co(II) cation was proven to be a suitable candidate for preparation of SIMs and SCMs.^{33–40} It exhibits high plasticity of the coordination sphere and strong enough spin-orbit coupling (SOC), which gives the possibility of magnetic anisotropy fine tuning. On the other hand, pseudohalide ions were found to be versatile ligands able to coordinate to metal centres in monodentate or bridging modes and generate mononuclear complexes or polymeric coordination networks.^{41–45} As demonstrated herein, the longer dca^- ions favoured the formation of a one dimensional network based on a single $\mu_{1,5}$ - dca bridge $[Co(pypz)(dca)(H_2O)]_n \cdot n(dca)$ (**1**). The azide ions also acted as bridges to form a dimer $[Co_2(pypz)_2(\mu_{1,1}-N_3)_2(N_3)_2] \cdot 2CH_3OH$ (**2**), while tcm^- counterbalanced the charge of $[Co(pypz)_2]^{2+}$ in $[Co(pypz)_2](tcm)_2$ (**3**).

Results and discussion

Synthesis and general characterization

The complexes $[Co(pypz)(dca)(H_2O)]_n \cdot n(dca)$ (**1**), $[Co_2(pypz)_2(\mu_{1,1}-N_3)_2(N_3)_2] \cdot 2CH_3OH$ (**2**), and $[Co(pypz)_2](tcm)_2$ (**3**) were obtained by reacting a methanol solution of $CoCl_2 \cdot 6H_2O$ and 2,6-bis(pyrazol-1-yl)pyridine (pypz) with a suitable pseudohalide ligand at room temperature. Detailed data about synthesis, analysis, and characterization are presented in the ESI†

The infrared spectra of **1–3** clearly show the presence of the pseudohalide ions and N-heterocyclic ligand (Fig. S1†). Intense stretching vibrations of dca^- ions in **1** appear as strong $\nu_s(C\equiv N)$ peaks in the region $2146–2173\text{ cm}^{-1}$ and weaker absorptions $\nu_{as} + \nu_s(C\equiv Ndca)$ and $\nu_{as}(C\equiv Ndca)$ in the range $2210–2316\text{ cm}^{-1}$. The occurrence of two peaks in the lower energy region (at 2173 and 2146 cm^{-1}) in the IR spectrum of **1** could be indicative of the presence of both bridging and uncoordinated dca^- in this compound. Also, the asymmetric stretching vibrations $\nu_{as}(N_3^-)$ occur as two close-lying peaks at 2094 and 2060 cm^{-1} . Also, the asymmetric stretching vibrations $\nu_{as}(N_3^-)$ occurring as two close-lying peaks at 2094 and 2060 cm^{-1} support two different coordination modes of the azido ligands in **2** (EO-bridging and terminal).^{46,47} The single and strong band $\nu_s(C\equiv N)$ at 2165 cm^{-1} in the IR spec-

trum of **3** confirms the presence of uncoordinated tcm^- ions in this compound. Compared to the absorption band for the salt $Ktcm$, it is only slightly blue-shifted. Medium intensity absorptions attributed to the stretching modes $\nu(C=N)$, and $\nu(C=C)$ of the pypz ligand occur in the range of $1343–1482\text{ cm}^{-1}$. The absorption band due to O–H stretching vibrations occurs at 3261 cm^{-1} (Fig. S1, ESI†).

To confirm the phase purity of the synthesized Co(II) complexes, the XRPD spectra of these compounds were recorded. As shown in Fig. S2–S4 (ESI†), the XRPD patterns measured for polycrystalline samples **1–3** were in good agreement with the XRPD patterns simulated from the respective single-crystal X-ray data using the Mercury program,⁴⁸ demonstrating that the crystal structures are truly representative of the bulk materials.

Structural description

The details concerning crystal data and refinement are summarized in Table S1.† The bond lengths and angles are gathered in Table S2 (see the ESI†).

[Co(pypz)(dca)(H₂O)]_n·n(dca) (**1**). The structure **1** is built up from the cationic linear chains $[Co(pypz)(\mu_{1,5}-dca)(H_2O)]_n^{n+}$ whose positive charge is counterbalanced by uncoordinated dca^- ions (Fig. 1a). The chains are linked into a supramolecu-

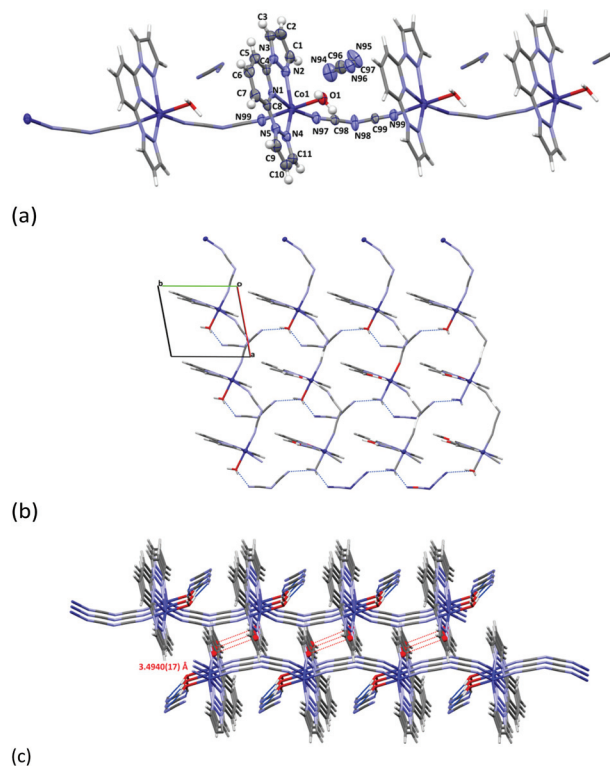
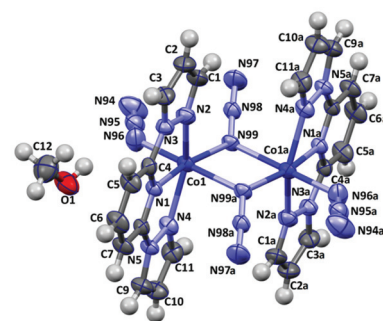


Fig. 1 (a) Perspective view of a fragment of the $[Co(pypz)(dca)(H_2O)]_n \cdot n(dca)$ showing the atom numbering. Displacement ellipsoids are drawn at 50% probability; (b) a view of a fragment of the supramolecular 2D network generated *via* hydrogen bonds; (c) a view of the supramolecular 3D network generated by interlayer π - π -stacking interactions involving the pypz ligands.

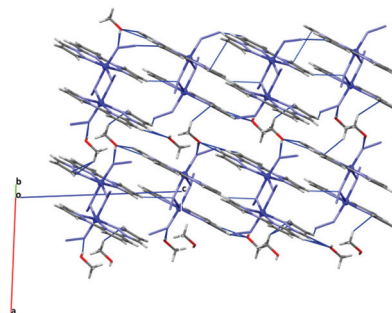
lar two-dimensional network *via* two structurally different O–H...N hydrogen bonds [(O(1)–H(1a)–N96; [D...A = 2.796(3) Å D–H...A = 172.0°] and O(1)–H(1b)–N94^b [D...A = 2.771(3) Å; D–H...A = 161.0°; (b): $x, 1 + y, z$]] (Fig. 1b). Neighbouring supramolecular layers are interlinked through π ... π stacking between the pyrazole rings of pypz ligands [3.4940(17) Å for Cg(4)(N(4)N(5)C(9)C(10)C(11)...Cg^c(4)(N(4)N(5)C(9)C(10)C(11)i) = $-x, 1 - y, -z$]. (Fig. 1c).

The shortest Co...Co separation spanned by the dca⁻ bridging ligand is 7.447(6) Å, while the closest interchain separation is equal to 8.4287(7) Å. Within the chain [Co(pypz)($\mu_{1,5}$ -dca)(H₂O)]_n²⁺, the adjacent metal centres are bridged by single $\mu^{1,5}$ -dca⁻ ligands, and each Co(II) atom has a six-coordinated CoN₅O environment, with a distorted octahedron coordination geometry. Three nitrogen atoms of the pypz ligand and one oxygen atom of the water molecule form the equatorial plane, while the axial position is occupied by two nitrogen atoms of bridging dca⁻ atoms. The cobalt(II) centre is displaced from the mean basal plane by 0.131 Å. The Shape value (OC-6) with respect to octahedral geometry was found to be 2.280, while the calculated distance to the ideal trigonal prism (TPR-6) is equal to 10.546.⁴⁹ The 2,6-bis(pyrazol-1-yl)pyridine skeleton is approximately planar. The dihedral angles between the inner and outer rings are 5.96(4)° and 1.33(4)°, respectively. Owing to the structural rigidity of the pypz ligand, the bond angles N(1)–Co(1)–N(2) (73.83(7)°) and N(1)–Co(1)–N(4) (74.17(7)°), are far off those expected for an ideal octahedral geometry. The Co–N bond of the central pyridyl ring of the pypz ligand [Co(1)–N(1) = 2.1082(18) Å] is shorter than those of the outer pyrazol-1-yl rings [Co(1)–N(2) = 2.1891(19) Å; Co(1)–N(4) = 2.1685(18) Å]. This trend has been also confirmed for the related Co(II) systems incorporating terpy and tppz ligands (see Table S3†). All the equatorial Co–N bond lengths are longer than the axial Co–Ndca bond lengths [Co(1)–N(97) = 2.057(2) Å; Co(1)–N(99) = 2.096(2) Å]. The elongation of the distance Co(1)–O(1) [2.1338(16) Å], compared to typical Co–O_{water} lengths for cobalt(II) complexes, can be explained by the participation of the oxygen atom in the formation of the intermolecular hydrogen bond O–H...N.^{50–52}

[Co₂(pypz)₂($\mu_{1,1}$ -N₃)₂(N₃)₂]-2CH₃OH (2). The structure 2 consists of the neutral dinuclear [Co₂(pypz)₂($\mu_{1,1}$ -N₃)₂(N₃)₂] entities and two molecules of methanol. The dinuclear unit results from the pairing of two mononuclear moieties related by a crystallographic inversion centre (Fig. 2a). The centrosymmetrically related Co(II) atoms are doubly bridged by azide ions in the end-on fashion to form a four-membered Co₂N₂ ring. The asymmetric ($\Delta d(\text{N–N}) = 0.161(1)$ Å) and quasi-linear (179.8(3)°) EO-bridging azido ligands are not coplanar with their Co₂N₂ ring. The intradimeric Co...Co separation of 3.3417(5) Å and the bridging angle Co(1)–N(99)–Co(1A) of 101.84(7)° agree well with the values reported previously for the related cobalt(II) dimers with double $\mu_{1,1}$ -N₃ bridges [see Table S4†]. However, it should be noted that the number of azido-bridged dinuclear cobalt(II) complexes is still limited, in contrast to dinuclear copper(II), manganese(II) and nickel(II) complexes with such bridges, on which extensive magnetostructural investigations have been reported.^{53–72}



a)



b)

Fig. 2 (a) Molecular structure of 2 together with the atom numbering. The displacement ellipsoids are drawn at 50% probability level [symmetry codes: (a) = $-x, -y, 2 - z$]; (b) a view of the supramolecular 2D network generated by hydrogen bonds.

Each Co(II) ion in 2 is in a distorted octahedral geometry consisting of three N atoms from pypz [Co(1)–N(1) = 2.0899(17) Å, Co(1)–N(2) = 2.1684(19) Å and Co(1)–N(4) = 2.1943(18) Å] and three other N atoms from the terminal and bridging azides [Co(1)–N(96) = 2.065(2) Å; Co(1)–N(99) = 2.0709(17) Å]. The Shape values with respect to octahedral geometry (OC-6) and trigonal prism (TBY-6) were found to be 2.300 and 10.954, respectively. The solvent molecules in the crystal structure of 2 are involved in the formation of the hydrogen bonds. The OH group of the methanol molecule is hydrogen bonded to the N(96) atom of the terminal azido ligand [O(1)–H(1A)...N(96) [D...A = 2.828(3) Å; D–H...A = 164.0°], C(3)–H(3)...O(1) [D...A = 3.162(3) Å; D–H...A = 163.0° (i): $x, 1/2 - y, 1/2 + z$], while the methanol oxygen atom participates in the weaker C–H...O interactions C(3)–H(3)...O(1) [D...A = 3.162(3) Å; D–H...A = 163.0° (i): $x, 1/2 - y, 1/2 + z$] and C(5)–H(5)...O(1) [D...A = 3.456(3) Å; D–H...A = 165.0°, (i): $x, 1/2 - y, 1/2 + z$], leading to a two-dimensional supramolecular network (Fig. 2b).

[Co(pypz)₂](tcm)₂ (3). Compound 3 crystallizes in the monoclinic space group *C2/c* with the asymmetric unit comprising one half of the [Co(pypz)₂]²⁺ cation and one tcm⁻ counterion. The Co(II) ion is situated on a twofold crystallographic axis. The perspective view of the molecular structure with the atom numbering is shown in Fig. 3. In the crystal structure, the cations [Co(pypz)₂]²⁺ and tcm⁻ anions are interlinked by electrostatic forces, weak hydrogen bonds C–H...N [C(1)–H(1)

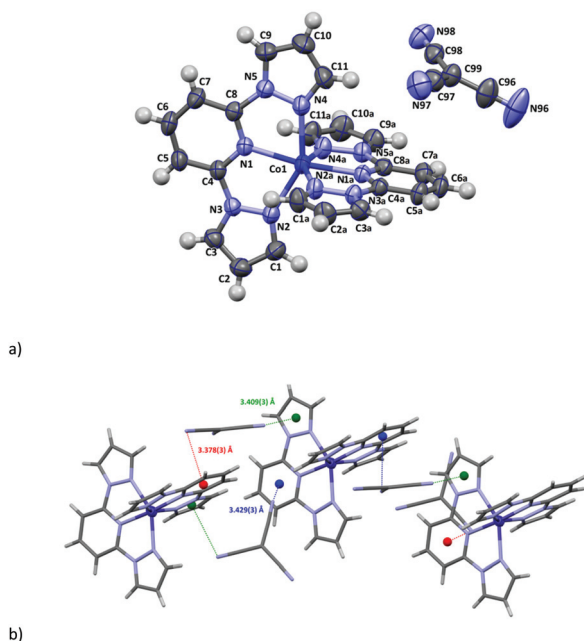


Fig. 3 (a) Molecular structure of **3** together with the atom numbering. The displacement ellipsoids are drawn at 50% probability level [symmetry codes: (h) = 1 - x, y, 3/2 - z]. (b) Short intermolecular contacts.

...N(98) D...A = 3.301(3) Å; D-H...A = 146.0° (f): 1 - x, -1 + y, 3/2 - z; C(5)-H(5)...N(96): D...A = 3.270(4) Å; D-H...A = 176.0° (g): 3/2 - x, 3/2 - y, 2 - z; C(7)-H(7)...N(98): D...A = 3.357(3) Å; D-H...A = 141.0° (g): 3/2 - x, -1/2 + y, 3/2 - z; C(11)-H(11)...N(97): D...A = 3.353(3) Å; D-H...A = 152.0°] and Y... π type interactions [C(98)-N(98)...Cg(7) X...Cg = 3.429(3) Å and C(97)-N(97)...Cg(7): X...Cg = 3.378(3) Å for centroids Cg7(N(1)-C(4)-C(5)-C(6)-C(7); C(96)-N(96)...Cg(6); X...Cg = 3.409(3) Å for centroids Cg6(N(4)-N(5)-C(9)-C(10)-C(11))].

In the cations $[\text{Co}(\text{pypz})_2]^{2+}$, the pypz ligands coordinate to the cobalt(II) ion in a *mer* fashion, equatorially *via* pyrazol-1-yl donors (Co(1)-N(2) = 2.1622(17) Å; Co(1)-N(4) = 2.1605(17) Å) and axially through the pyridyl nitrogen atoms (Co(1)-N(1) = 2.0825(14) Å), to form a tetragonally compressed $\{\text{CoN}_6\}$ octahedral symmetry. The Shape value for the octahedral environment (OC-6) was found to be 5.169, while the calculated value for ideal trigonal prism (TPR-6) is equal to 9.382. An angular distortion of $[\text{Co}(\text{pypz})_2]^{2+}$ which is reflected in the N-Co-N angles: 74.47(6)°-99.77(6)° for the nitrogen atoms in *cis* disposition and 148.72(6)°-171.72(8)° for those in *trans* arrangement is attributed to the rigidity and geometrical constraints related to the occurrence of two fused five-membered chelate rings of the pypz ligand. The dihedral angle between the least-squares planes formed by the pypz ligands is 89.49°. The distortion parameter Σ , defined as the sum of the deviation from 90° of the 12 *cis* angles of the CoN_6 octahedron, equals 141.47°, while the parameter θ being the summation of the 24 unique N-Co-N angles measured on the projection of two triangular faces of the octahedron along their common pseudo-threefold axis is 445°. The values of Σ and θ fall into the range typical of

HS cobalt(II) complexes.⁷³⁻⁷⁶ Also, the bond distances of Co-N (average Co-N = 2.1350(6) Å) clearly indicate the high-spin state (HS) of the cobalt(II) centre in $[\text{Co}(\text{pypz})_2]^{2+}$.⁷⁷⁻⁸⁰

DC magnetic data

The DC susceptibility data for **1** are displayed in Fig. 4. The effective magnetic moment at room temperature equals $\mu_{\text{eff}} = 5.17\mu_{\text{B}}$ which implies $g_{\text{eff}} = 2.67$. Its temperature dependence shows features typical of (nearly) octahedral Co(II) complexes with a pronounced maximum on cooling; at low temperature it is also influenced by the intermolecular interactions. The susceptibility increases on cooling over the whole temperature range, so that there is no evidence for an antiferromagnetic coupling along the 1D chain because of the absence of a maximum. The magnetization per formula unit reaches $M_1 = M_{\text{mol}}/N_A\mu_{\text{B}} = 2.87$ at $T = 2.0$ K and $B = 5.0$ T; this indicates a considerable zero-field splitting.

The geometry of the $\{\text{CoNN}'_2\text{N}''_2\text{O}\}$ chromophore is restricted by the rigid pypz ligand: the distance to the pyridine ring is shortened relative to the pyrazolate moiety but longer than distances to the dicyanamido ligands. The angular distortion is far from a right angle (as discussed above). Such a marked distortion from the octahedral geometry causes difficulties in selecting a suitable model Hamiltonian for fitting the magnetic data. On symmetry lowering the ground ${}^4\text{T}_{1g}(\text{O}_h)$ term is split into ${}^4\text{E}$ and ${}^4\text{A}_2$ daughter terms when assuming the C_{4v} geometry formed of the $\{\text{Co}(1)\text{N}(1)\text{N}(2)\text{N}(4)\text{N}(97)\}$ fragment (the C_4 axis passes throughout the O(1)-Co(1)-N(99) linkage). This symmetry descent could be described by the Griffith-Figgis (GF) Hamiltonian which is appropriate for the (quasi) degenerate ground term ${}^4\text{T}_{1g}$ on symmetry descent.

$$\hat{H}^{\text{GF}} = \underbrace{(-\lambda^{\text{sf}} A\kappa)}_{\text{spin-orbit coupling}} (\vec{L}_p \cdot \vec{S}) \hbar^{-2} + \underbrace{\mu_B \vec{B} \cdot (g_e \vec{S} + g_L \vec{L}_p)}_{\text{spin and orbital Zeeman terms}} \hbar^{-1} + \underbrace{\Delta_{\text{ax}} (\hat{L}_z^2 - \bar{L}^2/3)}_{\text{axial distortion}} \hbar^{-2} \quad (1)$$

The fitting procedure applied to magnetic susceptibility gave the following set of parameters: the effective spin-orbit splitting parameter $(A\kappa\lambda)/hc = -131(5) \text{ cm}^{-1}$, the effective orbital g -factor $g_L = -2.00(1)$, the axial crystal-field splitting parameter $\Delta_{\text{ax}}/hc = -2000 \text{ cm}^{-1}$; additional is the molecular

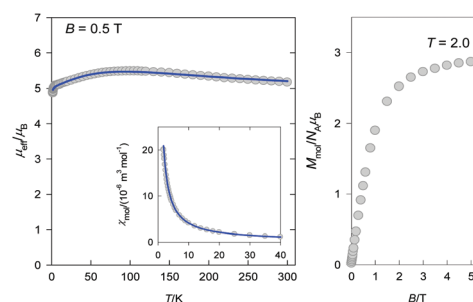


Fig. 4 DC magnetic data for **1**: effective magnetic moment (inset: low temperature susceptibility) and magnetization data. Full lines – fitted with the GF model.

field correction $(zj)/hc = -0.0057(14) \text{ cm}^{-1}$; the discrepancy factor $R(\chi) = 0.021$. (The last, minor correction improves the data fitting at the lowest temperatures.) The Griffith-Figgis model assumes a limiting value of $g_L > -1.5$; however, the fitting procedure with such a restriction failed. With $\Delta_{ax} \ll 0$, the ground term 4E is orbitally doubly degenerate so that four Kramers doublets are thermally populated and the spin-Hamiltonian formalism is not applicable. The larger deviation from the octahedron, the larger Δ_{ax} . There is no physical restriction for the magnitude of this splitting. Its large value says that the excited term 4A is magnetically ineffective.

Complex 2 is a dinuclear $S = 3/2$ spin system coupled in a ferromagnetic manner. The Co(1)–N(99)–Co(1A) bridge angle is 101.8° which lies close to the critical value at which the exchange interaction changes its sign.^{81–83} The room-temperature value of the effective magnetic moment is $\mu_{\text{eff}} = 7.87\mu_B$ (Fig. 5). The magnetic susceptibility on cooling is only increasing which indicates the ferromagnetic coupling. The magnetization per formula unit tends to saturate at $B = 7.0 \text{ T}$ & $T = 2.0 \text{ K}$ with $M_1 = 6.37$; this indicates a rather small value of the zero-field splitting parameter D .

The magnetic data were fitted by using the spin Hamiltonian

$$\hat{H}_a^{\text{SH}} = -J(\vec{S}_1 \cdot \vec{S}_2)\hbar^{-2} + \sum_{i=1}^2 D(\hat{S}_{i,z}^2 - \vec{S}_i^2/3)\hbar^{-2} + \sum_{i=1}^2 \mu_B B(g_z \hat{S}_{i,z} \cos \vartheta_a + g_{xy} \hat{S}_{i,x} \sin \vartheta_a)\hbar^{-1}$$

that accounts for the isotropic exchange (parameter J), zero-field splitting (parameter D), and the Zeeman term dependent upon a number of grids (a) along a meridian. The resulting parameters are: $J/hc = +17.8(7) \text{ cm}^{-1}$, $D/hc = 1.5 \text{ cm}^{-1}$, $g_z = g_{xy} = 2.50(1)$, temperature-independent term $\chi_{\text{TIM}} = -49 \times 10^{-9} \text{ m}^3 \text{ mol}^{-1}$; the discrepancy factors $R(\chi) = 0.014$.

Complex 3 is a mononuclear entity whose coordination polyhedron $\{\text{CoN}_4\text{N}'_2\}$ is a compressed octahedron. However, there is a considerable angular distortion caused by the rigidity of the pypz ligands. An analogous situation was encountered in the $[\text{Co}(\text{pydm})_2](\text{dnbz})_2$ complex formed from 2,6-pyridinedimethanol and dinitrobenzoate anions. A modelling using the generalized crystal field theory reveals that the angular distortion causes a crossover of the $A_2 \cdots E$ terms when

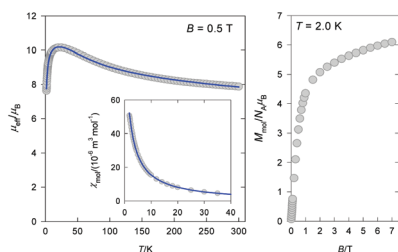


Fig. 5 DC magnetic data for 2: left – susceptibility data (inset: low temperature range), right – magnetization per formula unit. Lines – fitted.

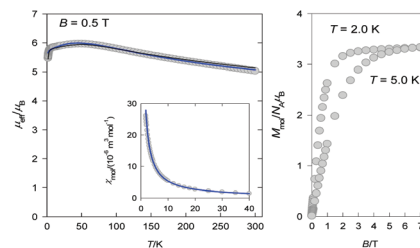


Fig. 6 DC magnetic data for 3: effective magnetic moment (inset: low temperature susceptibility) and magnetization data. Full lines – fitted with the GF model.

passing from D_{4h} to D_{2d} geometry.⁸⁴ Therefore, instead of the traditional zero-field splitting Hamiltonian, again the Griffith-Figgis model must be used (Fig. 6). The application of the Hamiltonian (1) gave $(A\kappa\lambda)/hc = -87(5) \text{ cm}^{-1}$, $g_L = -2.77(1)$, $\Delta_{ax}/hc = -4000 \text{ cm}^{-1}$, $(zj)/hc = -0.0049(15) \text{ cm}^{-1}$, and $\chi_{\text{TIM}} = -20 \times 10^{-9} \text{ m}^3 \text{ mol}^{-1}$; $R(\chi) = 0.031$. This set of parameters recovers the susceptibility data satisfactorily; however, the fitted values are a bit problematic (too low λ , too negative g_L).

Electron spin resonance

Cobalt(II) complexes in a hexacoordinated environment are often characterized by very large zero field splitting with the D parameter of the spin Hamiltonian often larger than 100 cm^{-1} and accordingly, only the transitions in the ground Kramers doublet $|\pm 1/2\rangle$ are observed (for a positive D). In cases where the spin Hamiltonian is applicable, this leads to a spectrum with an effective g_z value equal to the intrinsic g_z value, while the perpendicular g_{eff} values are approximately twice as large as the intrinsic g_x and g_y , still being dependent on the E/D ratio.⁸⁵ As shown above, the spin Hamiltonian is not applicable in our cases, since the complexes have orbitally degenerate ground states. Still, in the spectra of 1 and 3 some features are observed whose effective g -values are independent. These effective g -values are 7.20, 2.66 and 2.14 for 1 and 7.71, 1.84 and 1.47 for 3 (Fig. 7). The dimeric complex 2 exhibits very different spectra in which transitions located near to zero magnetic field are observed at multiple frequencies (Fig. 8). This is

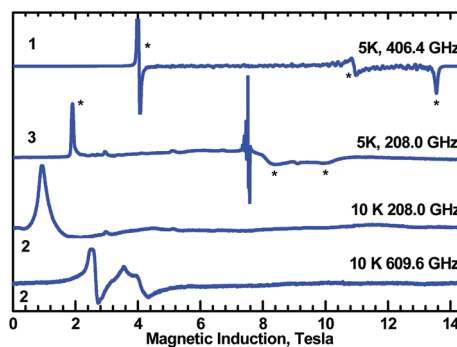


Fig. 7 High-field EPR spectra of complexes 1–3. The features marked with * in the spectra of 1 and 3 appear at the effective g -values which are independent of the microwave frequency.

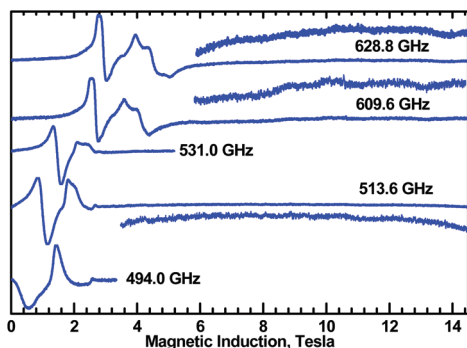


Fig. 8 High-field EPR spectra of **2** recorded at 10 K with the microwave frequencies as given. The lowest-field resonance appears at zero magnetic field when the frequency is 484 GHz.

indeed a signature of a dimeric compound and indicates some zero-field splitting.

When attempting to simulate the frequency dependencies of the resonances observed in **1** using $S = 3/2$ spin state with very large D and limiting $E/D = 1/3$, one obtains $g_x = 2.65$, $g_y = 2.61$ and $g_z = 2.95$. These g -values will change, however if a different E/D ratio is assumed. The lowest value of E/D which would not result in one of the g -values being smaller than 2 is 0.216, for which $g_x = 2$, $g_y = 2.80$ and $g_z = 2.45$ are required to fit the frequency dependencies in Fig. S5†. Such analysis proved to be impossible at all in the case of **3**, as it was impossible to simulate the frequency dependencies without some g -values being smaller than 2 (Fig. S6†).

Complex **2** exhibited complicated spectra with broad lines, particularly those occurring at high magnetic fields. The compound is a dinuclear $S = 3/2$ spin system coupled in a ferromagnetic manner with $J \sim +18 \text{ cm}^{-1}$. The coupled spin $S = 2$ state lies at 54 cm^{-1} above the ground $S = 3$ state, while the $S = 1$ state is $\sim 90 \text{ cm}^{-1}$ above $S = 3$. Therefore, at low temperatures only the coupled spin $S = 3$ state is expected to be observed in EPR. Transitions at or close to zero magnetic fields were observed at many microwave frequencies. A transition could be followed over a wide frequency range (Fig. S7†), which approached zero magnetic field at 484 GHz. This transition occurs between states which are split at zero field by 16 cm^{-1} (the factor to convert from cm^{-1} to GHz equals 30). The slope of that frequency dependence indicates that it is a $\Delta M_S = 1$ transition (plots of transitions with higher ΔM_S have lower slopes). The linearity of that branch in Fig. S7† suggests that it is a transition at the Z-orientation and allows estimation (from the slope) of $g_z = 2.0$. Neglecting the E parameter, the energies of the M_S states in $S = 3$ are 0, D , $4D$ and $9D$ for states $|0\rangle$, $|\pm 1\rangle$, $|\pm 2\rangle$ and $|\pm 3\rangle$, respectively. The $\Delta M_S = 1$ transitions at zero magnetic field in an $S = 3$ state occur at frequencies corresponding to D ($|0\rangle$ to $|\pm 1\rangle$), $3D$ ($|\pm 1\rangle$ to $|\pm 2\rangle$) and $5D$ ($|\pm 2\rangle$ to $|\pm 3\rangle$). The observed zero-field transition appears to be of the $5D$ type, thus D in the $S = 3$ state is estimated to be $\sim 3.2 \text{ cm}^{-1}$. This implies a D on a single Co^{2+} ion of 8 cm^{-1} , as a D_{Co} parameter on a single Co^{2+} ion contributes $0.4 D_{\text{Co}}$ to $D_{S=3}$, accord-

ing to the relation $\{D_{S=3}\} = 0.3\{D_{12}\} + 0.4\{D_{\text{Co}}\}$.⁸⁶ This is in disagreement with the magnetic data analysis and probably means that the standard spin Hamiltonian should not be applied to this system.

Quantum-chemical calculations

Ab initio calculations were performed with the ORCA 4.0.0 computational package⁸⁷ using the experimental geometry of complexes under study. The relativistic effects were included in the calculations with the zero-order regular approximation (ZORA) together with the scalar relativistic contracted version of def2-TZVPP basis functions for the Co atom, def2-TZVP basis functions for the N atom and def2-SV(P) basis functions for the C and H atoms. The calculations were based on the state average complete active space self-consistent field (SA-CASSCF) wave function complemented by N-electron valence second order perturbation theory (NEVPT2).^{88–92} The active space of the CASSCF calculations comprised of seven electrons in five metal-based d-orbitals. The state averaged approach was used, in which all 10 quartet and 40 doublet states were equally weighted. The calculations utilized the RI approximation with an appropriate decontracted auxiliary basis set and the chain-of-spheres (RIJCOSX) approximation to exact exchange. Increased integration grids (Grid4 and GridX5) and tight SCF convergence criteria were used. The spin-Hamiltonian parameters were evaluated through the quasi-degenerate perturbation theory in which an approximation to the Breit-Pauli form of the spin-orbit coupling operator (SOMF) and the effective Hamiltonian theory was utilized.^{93–95}

For the dinuclear complex **2**, the DFT-B3LYP calculation gave the exchange coupling constant $J/hc = +15.0 \text{ cm}^{-1}$ (Yamaguchi formula^{96,97}). The calculations utilized the RIJCOSX approximation with the auxiliary SARC/J Coulomb fitting basis set. Increased integration grids and tight SCF convergence criteria were also used.

In the mononuclear complex **3**, the three lowest lying multi-electron states (terms) can be considered as quasi-degenerate. These states arise from the splitting of the mother octahedral ground term ${}^4T_{1g}$ into daughter terms on symmetry lowering with energies ${}^4T_{1g}$: $\{0, 542, 1159\}$, hereafter all energy data in cm^{-1} . The remaining quartet terms lie at much higher energies, namely ${}^4T_{2g}$: $\{8693, 8764, 10\,572\}$; ${}^4A_{2g}$: $19\,164$; and ${}^4T_{1g}$: $\{21\,557, 23\,065, 23\,237\}$. The spin-orbit coupling splits the ground term into six multiplets (Kramers doublets) with energies $\{0, 163, 702, 992, 1474, 1601\}$. This means that the lowest energy gap amounts to $\delta = 163 \text{ cm}^{-1}$; however, this cannot be related to the traditional zero-field splitting parameter ($\delta \sim 2D$) since in the case of (quasi)degeneracy the spin-Hamiltonian formalism is inappropriate. Failure of the activated spin-Hamiltonian formalism is reflected in the calculated g -factors $g\{1.987, 2.334, 2.838\}$ where the first component acquires an unrealistic value (all g -factor components must be greater than 2 for d^7 systems). Consequently, the zero-field splitting parameters D and E are virtual and omitted from the presentation (in order to avoid any confusion).

AC susceptibility data

AC susceptibility data were acquired first at $T = 2.0$ K for a set of representative alternating field frequencies ($f = 1.1, 11, 1111$, and 1111 Hz), by increasing the magnetic field from zero to $B_{DC} = 1.0$ T. The working amplitude $B_{AC} = 0.3$ mT was used. Data for the complex **1** are displayed in the ESI.† There is no absorption signal (out-of-phase susceptibility component χ'') at the zero field owing to a fast magnetic tunnelling. With the increasing external field, this component rises, passes through a maximum, and then attenuates, which confirms that complex **1** exhibits a field supported slow magnetic relaxation. The position of the maximum, however, depends visibly on the oscillating field frequency, f . Complexes **2** and **3** exhibit analogous behaviour, which also demonstrates field induced slow magnetic relaxation.

Subsequent experiments were done for a fixed external magnetic field at which the high-frequency signal assumes a maximum. The data were taken for 22 oscillating field frequencies, between $f = 0.1$ and 1500 Hz, for a set of temperatures ranging between $T = 1.8$ and 7.0 K. These data were rearranged as shown in Fig. 9 for **1** where the frequency runs over the x -axis. There are two relaxation modes: (i) the low-frequency (LF) mode occurs at $f \sim 0.1$ Hz which implies the relaxation time $\tau(\text{LF}) = 1/(2\pi f_{\text{max}}) = 1.6$ s; (ii) the high-frequency (HF) mode refers to the peak at $f \sim 100$ Hz so that $\tau(\text{HF}) < 1.6$ ms at $T = 2.0$ K. The heights of the peaks, χ_{LF} and χ_{HF} , determine the mole fraction of the respective fraction *via* $\chi_{\text{LF}} = (\chi_{\text{LF}} - \chi_{\text{S}})/(\chi_{\text{HF}} - \chi_{\text{S}})$ where χ_{S} is the adiabatic susceptibility (the high-frequency limit). With increasing temperature x_{LF} decreases in favour of $x_{\text{HF}} = 1 - x_{\text{LF}}$. On heating, the position of the high-frequency peak is shifted to higher frequencies that is the usual behaviour of SMMs and SIMs. The AC susceptibility data were fitted by employing a two-set Debye model that can be decomposed into the pure real and imaginary parts (see the ESI† for details). Seven free parameters (adiabatic susceptibility χ_{S} , isothermal susceptibilities χ_{LF} , χ_{HF} , distribution parameters α_{LF} , α_{HF} , and relaxation times τ_{LF} , τ_{HF}) can be fitted reliably by using 44 experimental data points. The quality of the fit has been checked by the discrepancy factors $R(\chi')$ and $R(\chi'')$ along with standard deviations for each parameter (see

Table S5†). Note that the isothermal susceptibility defines the height of the peak, the distribution parameter its width, and the relaxation time the position of the peak at the out-of-phase susceptibility component. Normally, the α -parameter decreases on heating.

Based on quantitative assessment the relaxation time for the LF channel is as long as $\tau_{\text{LF}} = 1.8(7)$ s and that for the HF is $\tau_{\text{HF}} = 0.93(2)$ ms at $T = 2.0$ K, and $x_{\text{LF}} = 0.35$. The relaxation times enter the Arrhenius-like plot $\ln \tau$ vs. T^{-1} that is displayed in Fig. 10. This can be utilized in determining the relaxation parameters for the Orbach process in the high-temperature limit: the barrier to spin reversal $U/k_{\text{B}} = 103$ K. This value needs to be considered as an estimate since the maximum of the out-of-phase susceptibility component falls above the hardware limit (1500 Hz).

The curved part of the Arrhenius-like plot can be reproduced by considering a more general equation

$$\tau^{-1} = \tau_0^{-1} \exp(-U/k_{\text{B}}T) + CT^n + AB^m T + D_1/(1 + D_2 B^2) \quad (3)$$

in which also the multi-phonon Raman process (parameters C and n), the single-phonon direct process (parameters A and m) and the temperature-independent quantum tunnelling process are involved. The characteristic parameters can be estimated from the linearized form $\ln(\tau^{-1}) = b_0 + b_1 \ln T$ applied to different temperature windows. Two highest temperature points, ascribed to the Orbach relaxation process with $\tau = \tau_0 \exp(U/k_{\text{B}}T)$, gave $U/k_{\text{B}} = 103$ K, $\tau_0 = 1.2 \times 10^{-11}$ s. Here the barrier to spin reversal U is probably underestimated since the last three data points do not fall perfectly on the straight line and a hypothetical involvement of subsequent data points probably would bring a higher U and lower extrapolated relaxation time τ_0 . Six low-temperature data points match a linear relationship $\tau^{-1} = CT^n$ with $n = 1.3$ and $C = 426 \text{ K}^{-n} \text{ s}^{-1}$. Because $n > 1$, this refers to the Raman relaxation process; $n = 1$ would simulate the direct process and $n = 0$ the quantum tunnelling process. An almost perfect fit was obtained *via* truncated eqn (3) with parameters $U = 143(7)$ K, $\tau_0 = 1.6(13) \times 10^{-13}$ s, $AB^m = 1.3(1) \times 103 \text{ K}^{-1} \text{ s}^{-1} \text{ T}^{-m}$, $n = 5.7(2)$, and $C = 0.49(14)$

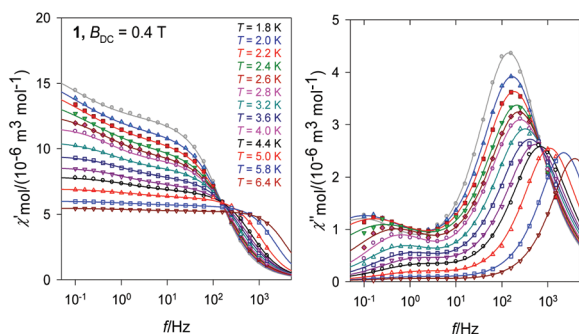


Fig. 9 Frequency dependence of the AC susceptibility components for **1** at $B_{DC} = 0.4$ T and fixed temperature. Lines – fitted with the two-set Debye model.

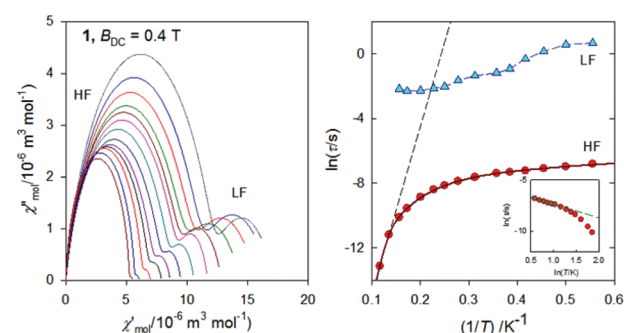


Fig. 10 Argand diagram (left) and the Arrhenius-like plot (right) for **1**. Orbach-process parameters in the high-temperature limit are $\tau = \tau_0 \exp(U/k_{\text{B}}T)$: $U/k_{\text{B}} = 103$ K, $\tau_0 = 1.2 \times 10^{-11}$ s. Raman (phonon bottleneck) process parameters in the low-temperature limit are $\tau^{-1} = CT^n$: $n = 1.3$, $C = 426 \text{ K}^{-n} \text{ s}^{-1}$ (inset).

$\text{K}^{-n} \text{s}^{-1}$. However, for the pure Raman process typical values are $n = 7-9$; subnormal n -values are more typical of the phonon bottleneck process which obeys an analogous formula.

The frequency dependence of the AC susceptibility components for **2** is shown in Fig. 11. Two peaks referring to the LF and HF relaxation processes are well seen. Again the two-set Debye model was successful in the data fitting. Despite the different chromophore and different structure motif, system **2** exhibits relaxation properties analogous to **1**: the relaxation time for the LF channel is as long as $\tau_{\text{LF}} = 1.5(2) \text{ s}$ and that for the HF is $\tau_{\text{HF}} = 0.82(3) \text{ ms}$ at $T = 2.0 \text{ K}$, and $\tau_{\text{LF}} = 0.36$. The adiabatic susceptibility is very different, however: zero is observed for **1** while it is substantial for **2**, escaping progressively with temperature. The shift of the adiabatic susceptibility is well seen in the Argand diagram drawn in Fig. 12.

The analysis of the Arrhenius-like plot gave the relaxation parameters for the high-temperature and the low-temperature regime as follows: $U/k_{\text{B}} = 95 \text{ K}$, $\tau_0 = 5.5 \times 10^{-15} \text{ s}$ for the Orbach process, and $n = 1.6$, $C = 412 \text{ K}^{-n} \text{ s}^{-1}$ for the Raman (phonon bottleneck) process. Again, a perfect fit has been obtained using eqn (3) with parameters $U = 83(8) \text{ K}$, $\tau_0 = 0.7 \times 10^{-13} \text{ s}$, $AB^m = 1.9(2) \times 10^3 \text{ K}^{-1} \text{ s}^{-1} \text{ T}^{-m}$, $n = 7.5(18)$ and $C = 0.43 \text{ K}^{-n} \text{ s}^{-1}$.

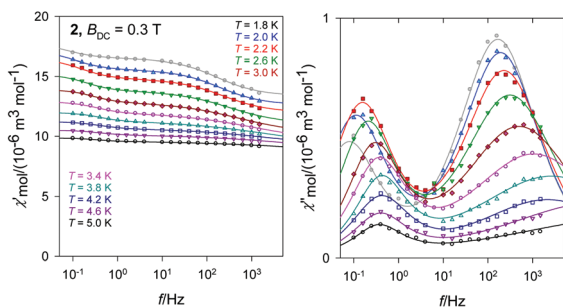


Fig. 11 Frequency dependence of the AC susceptibility components for **2** at $B_{\text{DC}} = 0.3 \text{ T}$ and fixed temperature. Lines – fitted with the two-set Debye model.

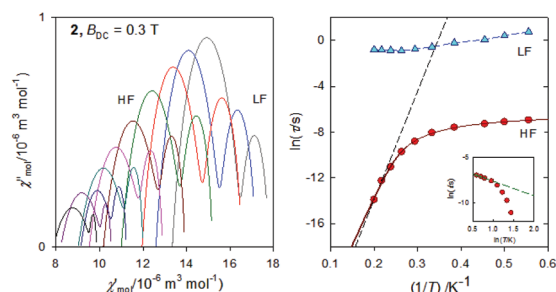


Fig. 12 Argand diagram (left) and the Arrhenius-like plot (right) for **2**. Orbach-process parameters in the high-temperature limit are $\tau = \tau_0 \exp(U/k_{\text{B}}T)$: $U/k_{\text{B}} = 95 \text{ K}$, $\tau_0 = 5.5 \times 10^{-15} \text{ s}$. Raman (phonon-bottleneck) process parameters in the low-temperature limit are $\tau^{-1} = CT^n$: $n = 1.6$, $C = 412 \text{ K}^{-n} \text{ s}^{-1}$ (inset).

The AC susceptibility data for **3** are different from the previous cases (Fig. 13 and 14). One dominating peak is seen at the out-of-phase component positioned at $f \sim 100 \text{ Hz}$ and above. Because of shoulders, the data fitting requires a three-set Debye model whose parameters are listed in Table S7.†

Multiple relaxation channels in mononuclear Co(II) based SIMs have been recognized in a number of studies.^{98–102} These systems possess aromatic rings and a rich system of short intermolecular contacts, like hydrogen bonds, π - π stacking, π -H interactions, *etc.* On heating, oligonuclear entities (blocks, plaquettes, and/or finite chains) relaxing slowly disintegrate to mononuclear (traditional) SIMs. Such an interpretation is supported by doping experiments into the diamagnetic Zn matrix. There is also a strong dependence of the LF relaxation channel upon the external magnetic field that acts as a “gluing” factor in the formation of the oligonuclear entities relaxing slowly.

The dynamic magnetic properties of three complexes under study can also be compared with analogous systems possessing hexacoordinated Co(II) ions (see Table 1). Many examples of such complexes presented in the literature exhibit SMM or SIM behaviour with one or two (sometimes three) relaxation modes and effective energy barriers for spin reversal typically in the range of 20–50 K. However, it should be noted that the spin-reversal barriers $U = 103 \text{ K}$ (**1**) or 95 K (**2**) are among the largest observed for other cobalt(II) field-induced SIMs or SMMs presented in the literature. This barrier to spin reversal which is responsible for the Orbach process of slow magnetic

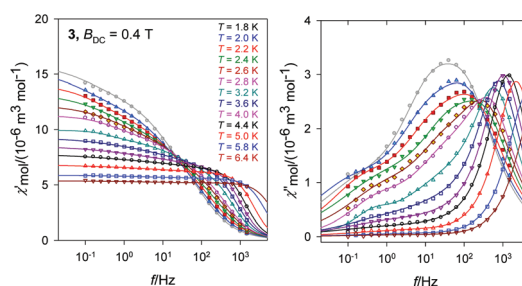


Fig. 13 Frequency dependence of the AC susceptibility components for **3** at $B_{\text{DC}} = 0.4 \text{ T}$ and fixed temperature. Lines – fitted with the three-set Debye model.

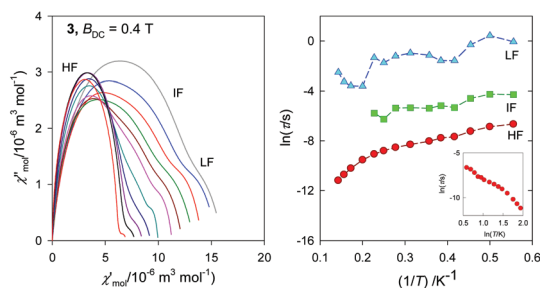


Fig. 14 Argand diagram (left) and the Arrhenius-like plot (right) for **3**. Dashed lines – guide to the eye.

Table 1 Comparison of the key characteristics of related complexes

Compound	$z'/hc/cm^{-1}$ $J/hc/cm^{-1}$	B_{DC}/T	Branch	$\tau(1.9\text{ K})/s$	$U/k_B/K$	τ_0/s	Ref.
$[\text{Co}(\text{bim})_4(\text{tcm})_2]^a$	~ 0	0.25			40.3		106
$[\text{Co}(\text{bmim})_4(\text{tcm})_2]^b$	~ 0	0.25			28.8		106
$[\text{Co}(\text{abpt})_2(\text{tcm})_2]^c$	0.3	0.3			86	1.4×10^{-9}	107
$[\text{Co}(4\text{-bzpy})_4\text{Cl}_2]^d$	-0.031	0.4	HF	273×10^{-6}			108
			IF	43.5×10^{-3}			
			LF	394×10^{-3}			
$[\text{Co}(4\text{-bzpy})_4(\text{SCN})_2]^d$	~ 0	0.4	HF	282×10^{-6}	27.7	0.31×10^{-6}	108
			LF	63.9×10^{-3}			
$[\text{Co}^{\text{II}}\text{Co}^{\text{III}}(\text{LH}_2)_2(\text{CH}_3\text{COO})(\text{H}_2\text{O})](\text{H}_2\text{O})_3]^e$	-0.069	0.4	HF	60.5×10^{-3}	24.4	0.59×10^{-6}	109
			LF	182×10^{-6}			
$[\text{Co}(\text{pypz})(\text{dca})(\text{H}_2\text{O})]_n \cdot n(\text{dca})$	-0.0057	0.4	HF	1.09×10^{-3}	103	1.2×10^{-11}	This work
			LF	1.9(7)			
$[\text{Co}_2(\text{pypz})_2(\text{N}_3)_2]$	-0.028	0.3	HF	0.95×10^{-3}	95	5.5×10^{-15}	This work
	+17.8(7)		LF	2.1(8)			
$[\text{Co}(\text{pypz})_2](\text{tcm})_2$	-0.0049	0.3	HF	1.3×10^{-3}			This work
			IF	13.7×10^{-3}			
			LF	0.9(11)			
$[\text{Co}(\text{pypz})\text{Cl}_2]$	-0.073	0.35	HF	237×10^{-6}	49	1.4×10^{-8}	85
			LF	0.93(13)			
$[\text{Co}(\text{pypz})(\text{NCS})_2]$	-0.029	0.40	HF	17.0×10^{-6}			85
			IF	3.0×10^{-3}			
			LF	4.9(24)			
$[\text{Co}(\text{pypz})(\text{NCO})_2]$	-0.019	0.20	HF	1.84×10^{-3}	25.3	4.5×10^{-7}	85
			LF	0.55(14)			

^a bim = 1-benzylimidazole. ^b bmim = 1-benzyl-2-methylbenzimidazole. ^c abpt = 4-amino-3,5-bis(2-pyridyl)-1,2,4-triazole; tcm = tricyanomethanide. ^d 4-bzpy = 4-benzylpyridine. ^e LH = 2-[[[2-hydroxy-3-methoxyphenyl)methylene]amino]-2-(hydroxymethyl)-1,3-propanediol.

relaxation is not always exclusively related to the D anisotropy parameter as $U = |D|(S^2 - 1/4)$. For example, our SIMs **1** (with a very high energy barrier) and **3**, which are both hexacoordinate Co(II) complexes with an elongated octahedral geometry, possess the orbitally (nearly) degenerate ground term (e.g. 4E) for which the spin-Hamiltonian formalism fails and thus the D -parameter is undefined. This fact was confirmed by magnetic and HF-EPR spectroscopic measurements and also theoretical calculations. Moreover, the large U value observed in the dimeric complex **2** does not meet the typical conditions assigned to SMM, such as a high spin and large negative D value. This Co(II) system possesses a positive and rather small D -value which may suggest that the occurrence and dynamics of relaxation processes depend on more varied and complex parameters. Angular distortion, steric effects, and short intermolecular contacts leading to dimer or chain formation can result in unpredictable deceleration or acceleration of slow magnetic relaxation. Note that also $S = \frac{1}{2}$ spin systems with undefined D -parameter can exhibit slow magnetic relaxation as documented by a few examples.^{103–105}

An additional value of our research is also demonstrating the role of a multicoordinate pypz ligand in the construction of SMM or SIM magnets. This ligand can act as a tridentate ligand and adopt various geometry modes (penta- or hexacoordinated) depending on the halogen or pseudohalogen anion (see Table 1). Introduction into the Co(II) coordination sphere of halido or pseudohalido ligands allows a fine-tuning and effective modulation of magnetic anisotropy, and consequently may lead to enhancement of the energy barrier. As a result all

complexes in our $[\text{Co}(\text{pypz})\text{X}_2]$ series where $\text{X} = \text{Cl}^-$, NCS^- , NCO^- , N_3^- , tcm^- , and dca^- show a field-induced relaxation process with two relaxation channels in **1**, **2** and $[\text{Co}(\text{pypz})\text{Cl}_2]$, $[\text{Co}(\text{pypz})(\text{NCO})_2]$ or three channels in **3** and $[\text{Co}(\text{pypz})(\text{NCS})_2]$, with an energy barrier much higher for the hexacoordinate than pentacoordinate Co(II) complexes. The strategy we use can be useful in constructing new magnetic materials with a great variety of structural motifs and interesting magnetic properties such as multichannel relaxation processes with a large energy barrier.

Conclusions

In summary, the effect of N-donor ligands in combination with halido or pseudohalido ligands on the construction of SMMs or SIMs was investigated. Three new Co(II) complexes with distorted octahedral geometries and different topologies have been synthesized and structurally characterized. The DC magnetic data show a sizable magnetic anisotropy, which was confirmed by HF EPR measurements and *ab initio* calculations.

The AC susceptibility measurements reveal that the hexacoordinate complexes **1** through **3** exhibit an exceptionally long relaxation time for the low-frequency channel upon application of an external field $B_{DC} = 0.4, 0.3$, and 0.4 T, respectively at low temperature $T = 1.9$ K: $\tau_{LF} = 1.9, 2.1$ and 0.9 s. These complexes exhibit the largest field-induced spin-reversal barrier among the cobalt(II) SIMs or SMMs. This barrier is not

exclusively related to the D anisotropy parameter, as due to the orbitally degenerate ground term the spin-Hamiltonian formalism fails and the D -parameter is undefined (1 and 3). The D -parameter adopts a very low and positive value in 2. This is an agreement with the thesis done by E. Ruiz *et al.*,¹¹⁰ that the magnitude of the anisotropy barrier in SMM is mainly determined by the strength of the spin-orbit coupling and cannot be engineered by independently optimizing D and S . Further studies on cobalt(II), nickel(II) and manganese(II) complexes using 2,6-bis(pyrazol-1-yl)pyridine and halido or pseudohalido ligands will be carried out in the near future in order to investigate the relationship between the substitution pattern/steric effects and the relaxation dynamics of these relatively simple anisotropic systems.

Conflicts of interest

There is no conflict to declare.

Acknowledgements

This work was supported by the Polish National Science Centre (grant no. 2015/17/D/ST5/01344; A. Ś). Slovak grant agencies (APVV-18-0016, APVV 16-0039, VEGA 1/0919/17 and VEGA 1/0534/16; R. B.) are acknowledged for the financial support. The high-field EPR spectra were recorded at the NHMFL, which is funded by the NSF through the Cooperative Agreement No. DMR-1644779 and the State of Florida. (A. O.).

References

- R. Sessoli, D. Gatteschi, A. Caneschi and M. A. Novak, Magnetic bistability in a metal-ion cluster, *Nature*, 1993, **365**, 141.
- L. Váhovská, S. Vitushkina, I. Potočňák, Z. Trávníček and R. Herchel, Effect of linear and non-linear pseudohalides on the structural and magnetic properties of Co(II) hexacoordinate single-molecule magnets, *Dalton Trans.*, 2018, **47**, 1498.
- J. Ferrando-Soria, J. Vallejo, M. Castellano, J. Martínez-Lillo, E. Pardo, J. Cano, I. Castro, F. Lloret, R. Ruiz-García and M. Julve, Molecular magnetism, quo vadis? A historical perspective from a coordination chemist viewpoint, *Coord. Chem. Rev.*, 2017, **339**, 17.
- F. D. Natterer, K. Yang, W. Paul, P. Willke, T. Choi, T. Greber, A. J. Heinrich and C. P. Lutz, Reading and writing single-atom magnets, *Nature*, 2017, **543**, 226.
- F. Donati, S. Rusponi, S. Stepanow, C. Wäckerlin, A. Singha, L. Persichetti, R. Baltic, K. Diller, F. Patthey, E. Fernandes, J. Dreiser, Ž Šljivančanin, K. Kummer, C. Nistor, P. Gambardella and H. Brune, Magnetic remanence in single atoms, *Science*, 2016, **352**, 318.
- A. Gaita-Arino, H. Prima-Garcia, S. Cardona-Serra, L. Escalera-Moreno, L. E. Rosaleny and J. J. Baldovi, Coherence and organisation in lanthanoid complexes: from single ion magnets to spin qubit, *Inorg. Chem. Front.*, 2016, **3**, 568.
- S. Dhers, H. L. C. Feltham and S. Brooker, A toolbox of building blocks, linkers and crystallisation methods used to generate single-chain magnets, *Coord. Chem. Rev.*, 2015, **296**, 24.
- J. S. Miller and D. Gatteschi, Molecule-based magnets, *Chem. Soc. Rev.*, 2011, **40**, 3065.
- L. Bogani and W. Wernsdorfer, Molecular Spintronics Using Single-Molecule Magnets, *Nat. Mater.*, 2008, **7**, 179.
- J. H. Jia, Q. W. Li, Y. C. Chen, J. L. Liu and M. L. Tong, Luminescent single-molecule magnets based on lanthanides: Design strategies, recent advances and magneto-luminescent studies, *Coord. Chem. Rev.*, 2019, **378**, 365.
- S. G. McAdams, A. M. Ariciu, A. K. Kostopoulos, J. P. S. Walsh and F. Tuna, Molecular single-ion magnets based on lanthanides and actinides: Design considerations and new advances in the context of quantum technologies, *Coord. Chem. Rev.*, 2017, **346**, 216.
- F. Pointillart, O. Cador, B. Le Guennic and L. Ouahab, Uncommon lanthanide ions in purely 4f Single Molecule Magnets, *Coord. Chem. Rev.*, 2017, **346**, 150.
- K. Liu, X. Zhang, X. Meng, W. Shi, P. Cheng and A. K. Powell, Constraining the coordination geometries of lanthanide centers and magnetic building blocks in frameworks: a new strategy for molecular nanomagnets, *Chem. Soc. Rev.*, 2016, **45**, 2423.
- J. M. Frost, K. L. Harriman and M. Murugesu, The rise of 3-d single-ion magnets in molecular magnetism: towards materials from molecules?, *Chem. Sci.*, 2016, **7**, 2470.
- G. A. Craig and M. Murrie, 3d single-ion magnets, *Chem. Soc. Rev.*, 2015, **44**, 2135.
- A. Pascual-Álvarez, J. Vallejo, E. Pardo, M. Julve, F. Lloret, J. Krzystek, D. Armentano, W. Wernsdorfer and J. Cano, Field-Induced Slow Magnetic Relaxation in a Mononuclear Manganese(III)-Porphyrin Complex, *Chem. – Eur. J.*, 2015, **21**, 17299.
- L. R. Piquer and E. C. Sañudo, Heterometallic 3d–4f single-molecule magnets, *Dalton Trans.*, 2015, **44**, 8771.
- L. Zhang, Y. Q. Zhang, P. Zhang, L. Zhao, M. Guo and J. Tang, Single-Molecule Magnet Behavior Enhanced by Synergic Effect of Single-Ion Anisotropy and Magnetic Interactions, *Inorg. Chem.*, 2017, **56**, 7882.
- M. Bohme and W. Plass, How to link theory and experiment for single-chain magnets beyond the Ising model: magnetic properties modeled from *ab initio* calculations of molecular fragments, *Chem. Sci.*, 2019, **10**, 9189.
- S. Dhers, H. L. C. Feltham, M. Rouzières, R. Clérac and S. Brooker, Discrete versus Chain Assembly: Hexacyanometallate Linkers and Macrocyclic {3d–4f} Single-Molecule Magnet Building Blocks, *Inorg. Chem.*, 2019, **58**, 5543.
- A. Kawamura, A. S. Filatov, J. S. Anderson and I.-R. Jeon, Slow Magnetic Relaxation of Co(II) Single Chains

- Embedded within Metal–Organic Superstructures, *Inorg. Chem.*, 2019, **58**(6), 3764.
- 22 Y. Z. Zhang, B. S. Dolinar, S. Liu, A. J. Brown, X. Zhang, Z. X. Wang and K. R. Dunbar, Enforcing Ising-like magnetic anisotropy *via* trigonal distortion in the design of a W(V)–Co(II) cyanide single-chain magnet, *Chem. Sci.*, 2018, **9**, 119.
- 23 J. Werner, M. Rams, Z. Tomkowicz, T. Runčevski, R. E. Dinnebier, S. Suckert and C. Näther, Thermodynamically Metastable Thiocyanato Coordination Polymer That Shows Slow Relaxations of the Magnetization, *Inorg. Chem.*, 2015, **54**, 2893.
- 24 M. Rams, M. Böhme, V. Kataev, Y. Krupskaya, B. Büchner, W. Plass, T. Neumann, Z. Tomkowicz and C. Näther, Static and dynamic magnetic properties of the ferromagnetic coordination polymer [Co(NCS)₂(py)₂]_n, *Phys. Chem. Chem. Phys.*, 2017, **19**, 24534.
- 25 B. Drahoš, R. Herchel and Z. Trávníček, Single-Chain Magnet Based on 1D Polymeric Azido-Bridged Seven Coordinate Fe(II) Complex with a Pyridine-Based Macrocyclic Ligand, *Inorg. Chem.*, 2018, **57**, 12718.
- 26 A. K. Bar, C. Pichon and J. P. Sutter, Magnetic anisotropy in two- to eight-coordinated transition–metal complexes: Recent developments in molecular magnetism, *Coord. Chem. Rev.*, 2016, **308**, 346.
- 27 M. G. Pini, A. Rettori, L. Bogani, A. Lascialfari, M. Mariani, A. Caneschi and R. Sessoli, Finite-size effects on the dynamic susceptibility of CoPhOMe single-chain molecular magnets in presence of a static magnetic field, *Phys. Rev. B: Condens. Matter Mater. Phys.*, 2011, **84**, 094444.
- 28 M. Murrie, Cobalt(II) single-molecule magnets, *Chem. Soc. Rev.*, 2010, **39**, 1986.
- 29 H. A. Kramers, *Proc. Rochester Acad. Sci.*, 1930, **33**, 959.
- 30 S. Vaidya, S. Tewary, S. K. Singh, S. K. Langley, K. S. Murray, Y. Lan, W. Wernsdorfer, G. Rajaraman and M. Shanmugam, What Controls the Sign and Magnitude of Magnetic Anisotropy in Tetrahedral Cobalt(II) Single-Ion Magnets?, *Inorg. Chem.*, 2016, **55**, 9564.
- 31 S. Gomez-Coca, A. Urtizberea, E. Cremades, P. J. Alonso, A. Camon, E. Ruiz and F. Luis, Origin of slow magnetic relaxation in Kramers ions with non-uniaxial anisotropy, *Nat. Commun.*, 2014, **5**, 4300.
- 32 Z.-W. Chen, L. Yin, X. N. Mi, S. N. Wang, F. Cao, Z. X. Wang, Y. W. Li, J. Lu and J. M. Dou, Field-induced slow magnetic relaxation of two 1-D compounds containing six-coordinated cobalt(II) ions: influence of the coordination geometry, *Inorg. Chem. Front.*, 2018, **5**, 2314.
- 33 A. K. Mondal, J. Jover, E. Ruiz and S. Konar, Single-ion magnetic anisotropy in a vacant octahedral Co(II) complex, *Dalton Trans.*, 2019, **48**, 25.
- 34 J. Vallejo, M. Viciano-Chumillas, F. Lloret, M. Julve, I. Castro, J. Krzystek, M. Ozerov, D. Armentano, G. De Munno and J. Cano, Coligand Effects on the Field-Induced Double Slow Magnetic Relaxation in Six-Coordinate Cobalt(II) Single-Ion Magnets (SIMs) with Positive Magnetic Anisotropy, *Inorg. Chem.*, 2019, **58**, 15726.
- 35 S. Tripathi, S. Vaidya, K. U. Ansari, N. Ahmed, E. Rivière, L. Spillecke, C. Koo, R. Klingeler, T. Mallah, G. Rajaraman and M. Shanmugam, Influence of a Counteranion on the Zero-Field Splitting of Tetrahedral Cobalt(II) Thiourea Complexes, *Inorg. Chem.*, 2019, **58**, 9085.
- 36 R. Bruno, J. Vallejo, N. Marino, G. De Munno, J. Krzystek, J. Cano, E. Pardo and D. Armentano, Cytosine Nucleobase Ligand: A Suitable Choice for Modulating Magnetic Anisotropy in Tetrahedrally Coordinated Mononuclear Co^{II} Compounds, *Inorg. Chem.*, 2017, **56**, 1857.
- 37 J. Palion-Gazda, B. Machura, R. Kruszynski, T. Grancha, N. Moliner, F. Lloret and M. Julve, Spin Crossover in Double Salts Containing Six- and Four-Coordinate Cobalt (II) Ions, *Inorg. Chem.*, 2017, **56**, 6281.
- 38 J. Vallejo, E. Pardo, M. Viciano-Chumillas, I. Castro, P. Amorós, M. Déniz, M. Ruiz-Pérez, C. Yuste-Vivas, J. Krzystek, M. Julve, F. Lloret and J. Cano, Reversible solvatomagnetic switching in a single-ion magnet from an entatic state, *Chem. Sci.*, 2017, **8**, 3694.
- 39 G. Brunet, D. A. Safin, J. Jover, E. Ruiz and M. Murugesu, Single-molecule magnetism arising from cobalt(II) nodes of a crystalline sponge, *J. Mater. Chem. C*, 2017, **5**, 835.
- 40 L. Sun, S. Zhang, S. Chen, B. Yin, Y. Sun, Z. Wang, Z. Ouyang, J. Ren, W. Wang, Q. Wei, G. Xie and S. Gao, A two-dimensional cobalt(II) network with a remarkable positive axial anisotropy parameter exhibiting field-induced single-ion magnet behavior, *J. Mater. Chem. C*, 2016, **4**, 7798.
- 41 A. Escuer, J. Esteban, S. P. Perlepes and T. C. Stamatatos, The bridging azido ligand as a central “player” in high-nuclearity 3d-metal cluster chemistry, *Coord. Chem. Rev.*, 2014, **275**, 87.
- 42 P. Portius and M. Davis, Recent developments in the chemistry of homoleptic azido complexes of the main group elements, *Coord. Chem. Rev.*, 2013, **257**, 1011.
- 43 C. Adhikary and S. Koner, Structural and magnetic studies on copper(II) azido complexes, *Coord. Chem. Rev.*, 2010, **254**, 2933.
- 44 S. R. Batten and K. S. Murray, Structure and magnetism of coordination polymers containing dicyanamide and tri-cyanomethanide, *Coord. Chem. Rev.*, 2003, **246**, 103.
- 45 J. S. Miller and J. L. Manson, Designer Magnets Containing Cyanides and Nitriles, *Acc. Chem. Res.*, 2001, **34**, 563.
- 46 S. S. Tandon, L. K. Thompson, M. E. Manuel and J. N. Bridson, Magnetostructural Correlations in μ_2 -1,1- N_3 Bridged, Dinuclear Copper(II) Complexes. 1. Ferromagnetic and Antiferromagnetic Coupling Associated with the Azide Bridge. X-ray Crystal Structures of [Cu₂(DMPTD)(μ_2 -N₃)(μ_2 -Cl)Cl₂].CH₃CN, [Cu₂(DMPTD)(μ_2 -N₃)₂(N₃)₂], [Cu₂(DIP)(μ_2 -N₃)(μ_2 -Cl)Cl₂].0.5CH₃OH, [Cu₂(PAP₄Me-H)(μ_2 -N₃)(N₃)₂].0.33H₂O, [Cu₂(PAP) μ_2 -N₃Cl₃].CH₂Cl₂, [Cu₂(PAP)(μ_2 -N₃)(N₃)(NO₃)(CH₃OH)](NO₃).CH₃OH, [Cu₂(PPD3Me)(μ_2 -N₃)

- $Cl_3(H_2O)_{1.5}]$ and $[Cu_2(PPD)_{\mu_2-N_3}(NO_3)_3(H_2O)_{1.6}]$, *Inorg. Chem.*, 1994, **33**, 5555.
- 47 X. Wang, Y. H. Xing, F. Y. Bai, X. Y. Wang, Q. L. Guan, Y. N. Hou, R. Zhang and Z. Shi, Synthesis, structure, and surface photovoltage properties of a series of novel d^7-d^{10} metal complexes with pincer N-heterocycle ligands, *RSC Adv.*, 2013, **3**, 16021.
- 48 C. F. Macrae, I. J. Bruno, J. A. Chisholm, P. R. Edfinton, P. McCabe, E. Pidcock, L. Rodriguez-Monge, R. Taylor, J. van de Streek and P. A. Wood, Mercury CSD 2.0 – new features for the visualization and investigation of crystal structures, *J. Appl. Crystallogr.*, 2008, **41**, 466.
- 49 M. Llunell, D. Casanova, J. Cirera and P. Alemany and S. Alvarez, *S. SHAPE version 2.0*, Universitat de Barcelona, 2010.
- 50 J. Luo, L. Qiu, B. Liu, X. Zhang, F. Yang and L. Cui, Synthesis, Structure and Magnetic Properties of Two Cobalt(II) Dicyanamide (dca) Complexes with Heterocyclic Nitrogen Donors Tetra(2-pyridyl)pyrazine (tppz) and 2,4,6-Tri(2-pyridyl)-1,3,5-triazine (tptz): $[Co_2(tppz)(dca)_4] \cdot CH_3CN$ and $[Co(tptz)(dca)(H_2O)](dca)$, *Chin. J. Chem.*, 2012, **30**, 522.
- 51 S. R. Marshall, C. D. Incarvito, J. L. Manson, A. L. Rheingold and J. S. Miller, Synthesis, Structure, and Magnetic Properties of $Co_2\{[N(CN)_2]_4bpym\} \cdot H_2O$ and $M\{[N(CN)_2]_2bpym\} \cdot H_2O$ (M=Mn, Fe, Co; bpym=2,2'-Bipyrimidine), *Inorg. Chem.*, 2000, **39**, 1969.
- 52 P. Jensen, S. R. Batten, B. Moubaraki and K. S. Murray, Syntheses, crystal structures, and magnetic properties of first row transition metal coordination polymers containing dicyanamide and 4,4'-bipyridine, *J. Chem. Soc., Dalton Trans.*, 2002, 3712.
- 53 T. K. Karmakar, B. K. Ghosh, A. Usman, H. K. Fun, E. Riviere, T. Mallah, G. Aromi and S. K. Chandra, Magneto-Structural Correlations: Synthesis of a Family of End-On Azido-Bridged Manganese(II) Dinuclear Compounds with S=5 Spin Ground State, *Inorg. Chem.*, 2005, **44**, 2391.
- 54 Z. H. Ni, H. Z. Kou, L. Zheng, Y. H. Zhao, L. F. Zhang, R. J. Wang, A. L. Cui and O. Sato, Assembly of Azido- or Cyano-Bridged Binuclear Complexes Containing the Bulky $[Mn(phen)_2]^{2+}$ Building Block: Syntheses, Crystal Structures, and Magnetic Properties, *Inorg. Chem.*, 2005, **44**, 4728.
- 55 Z. S. Meng, L. Yun, W. X. Zhang, C. G. Hong, R. Herchel, Y. C. Ou, J. D. Leng, M. X. Peng, Z. J. Lin and M. J. Tong, Reactivity of 4-amino-3,5-bis(pyridin-2-yl)-1,2,4-triazole, structures and magnetic properties of polynuclear and polymeric Mn(II), Cu(II) and Cd(II) complexes, *Dalton Trans.*, 2009, 10284.
- 56 C. F. Wang, G. L. Dai, Z. N. Jin and Z. C. He, Synthesis, Structure, and Supramolecular Chemistry of Three Azide Manganese Complexes with 2, 6-Bis(benzimidazol-2-yl)pyridine, *Z. Anorg. Allg. Chem.*, 2012, **638**, 1340.
- 57 J. P. Zhao, R. Zhao, Q. Yang, B. W. Hu, F. C. Liu and X. H. Bu, Magnetocaloric effect and slow magnetic relaxation in two only azido bridged ferromagnetic tetranuclear metal clusters, *Dalton Trans.*, 2013, **42**, 14509.
- 58 J. Chaignon, S. E. Stiriba, F. Lloret, C. Yuste, G. Pilet, L. Bonneviot, B. Albela and I. Castro, Bioinspired manganese(II) complexes with a clickable ligand for immobilisation on a solid support, *Dalton Trans.*, 2014, **43**, 9704.
- 59 R. Cortes, J. I. R. de Larramendi, L. Lezama, T. Rojo, K. Urriaga and M. I. Arriortua, Synthesis, structural, spectroscopic and magnetic studies of two azido and thiocyanato nickel(II) dinuclear complexes with ferromagnetic interactions, *J. Chem. Soc. Dalton Trans.*, 1992, 2723.
- 60 R. Vicente, A. Escuer, I. Ribas, M. Salah el Fallah, X. Solans and M. Font-Bardia, New dinuclear penta- and hexacoordinated nickel(II) complexes with μ -azido bridges. Crystal structures of ferromagnetically coupled $(\mu-N_3)_2[Ni(Me_3[12]N_3)]_2(ClO_4)_2 \cdot 2H_2O$ and $(\mu-N_3)_2[Ni(232-N_4)]_2(ClO_4)$, *Inorg. Chem.*, 1993, **32**, 1920.
- 61 J. Ribas, M. Monfort, C. Diaz, C. Bastos and X. Solans, Ferromagnetic nickel(II) polynuclear complexes with end-on azido as bridging ligand. The first nickel(II)-azido one-dimensional ferromagnetic systems, *Inorg. Chem.*, 1994, **33**, 484.
- 62 A. Escuer, R. Vicente, J. Ribas and X. Solans, Magnetic Transition and Structural Asymmetrization in the Ferromagnetic Compound $[\{Ni_2(Medpt)_2(N_3)_2\}(\mu-(1,1-N_3)_2)]$, an Example of a Dynamic Second-Order Jahn-Teller Effect, *Inorg. Chem.*, 1995, **34**, 1793.
- 63 P. D. Beer, M. G. B. Drew, P. B. Leeson, K. Lyssenko and M. I. Ogden, A novel bis(N,N'-dimethyl-1,4,7-triazacyclononane)calyx[4]arene ligand that forms a ferromagnetic dinuclear nickel(II) complex with three end-on azide bridging ligands, *J. Chem. Soc., Chem. Commun.*, 1995, 929.
- 64 M. G. Barandika, R. Cortes, L. Lezama, M. K. Urriaga, M. I. Arriortua and T. Rojo, Synthesis and magnetostructural characterization of two ferromagnetic nickel(II) dimers, *J. Chem. Soc., Dalton Trans.*, 1999, 2971.
- 65 R. Kurtaran, C. Arici, K. C. Emregul, D. Ulku, O. Atakol and M. Tastekin, Synthesis, Crystal Structure, and Electrochemical Behaviour of an Azido μ -bridged Ni^{+2} Complex, *Z. Anorg. Allg. Chem.*, 2003, **629**, 1617.
- 66 S. K. Dey, N. Mondal, M. S. El Fallah, R. Vicente, A. Escuer, X. Solans, M. Font-Bardia, T. Matsushita, V. Gramlich and S. Mitra, Crystal Structure and Magnetic Interactions in Nickel(II) Dibridged Complexes Formed by Two Azide Groups or by Both Phenolate Oxygen-Azide, -Thiocyanate, -Carboxylate, or -Cyanate Groups, *Inorg. Chem.*, 2004, **43**, 2427.
- 67 M. L. Tong, C. G. Hong, L. L. Zheng, M. X. Peng, A. Gaitarino and J. M. C. Juan, New Reactivity of 4-Amino-3,5-bis(pyridin-2-yl)-1,2,4-triazole: Synthesis and Structure of a Mononuclear Species, a Dinuclear Species, and a Novel Tetranuclear Nickel(II) Rectangle Box, and Magnetic Properties of the Dinuclear and Tetranuclear Complexes, *Eur. J. Inorg. Chem.*, 2007, 3710.
- 68 M. Habib, T. K. Karmakar, G. Aromi, J. Ribas-Arino, H. K. Fun, S. Chantrapromma and S. K. Chandra, A

- Versatile Series of Nickel(II) Complexes Derived from Tetradentate Imine/Pyridyl Ligands and Various Pseudohalides: Azide and Cyanate Compared, *Inorg. Chem.*, 2008, **47**, 4109.
- 69 S. S. Massoud, F. R. Louka, Y. K. Obaid, R. Vicente, J. Ribas, R. C. Fischer and F. A. Mautner, Metal ions directing the geometry and nuclearity of azido-metal(II) complexes derived from bis(2-(3,5-dimethyl-1H-pyrazol-1-yl)ethyl)amine, *Dalton Trans.*, 2013, **42**, 3968.
- 70 X. Wang, Y. H. Xing, F. Y. Bai, X. Y. Wang, Q. L. Guan, Y. N. Hou, R. Zhang and Z. Shi, Synthesis, structure, and surface photovoltage properties of a series of novel d^7-d^{10} metal complexes with pincer N-heterocycle ligands, *RSC Adv.*, 2013, **3**, 16021.
- 71 C. Adhikary and S. Koner, Structural and magnetic studies on copper(II) azido complexes, *Coord. Chem. Rev.*, 2010, **254**, 2993.
- 72 J. Ribas, A. Escuer, M. Monfort, R. Vicente, R. Cortés, L. Lezama and T. Rojo, *Coord. Chem. Rev.*, 1999, **193–195**, 1027.
- 73 Y. Guo, X. L. Yang, R. J. Wei, L. S. Zheng and J. Tao, Spin Transition and Structural Transformation in a Mononuclear Cobalt(II) Complex, *Inorg. Chem.*, 2015, **54**, 7670.
- 74 H. Oshio, H. Spiering, V. Ksenofontov, F. Renz and P. Gütllich, Electronic Relaxation Phenomena Following $^{57}\text{Co}(\text{EC})$ ^{57}Fe Nuclear Decay in $[\text{Mn}^{\text{II}}(\text{terpy})_2](\text{ClO}_4)_2 \cdot 1/2\text{H}_2\text{O}$ and in the Spin Crossover Complexes $[\text{Co}^{\text{II}}(\text{terpy})_2]\text{X}_2 \cdot n\text{H}_2\text{O}$ (X=Cl and ClO_4): A Mössbauer Emission Spectroscopic Study, *Inorg. Chem.*, 2001, **40**, 1143.
- 75 A. Galet, A. B. Gaspar, M. C. Muñoz and J. A. Real, Void Geometry Driven Spin Crossover in Zeolite-Encapsulated Cobalt Tris(bipyridyl) Complex Ion, *Inorg. Chem.*, 2006, **45**, 4413.
- 76 R. G. Miller and S. Brooker, Reversible Redox, and Supramolecular Interactions in 3d Complexes of 4-(4-Pyridyl)-2,5-dipyrazyl-pyridine, *Inorg. Chem.*, 2015, **54**, 5398.
- 77 J. Luo, X. R. Zhang, L. J. Qiu, B. S. Liu and Z. Y. Zhang, Bis(2,2':6',2''-terpyridine)cobalt(II) bis(tricyanomethanide), *Acta Crystallogr., Sect. E: Struct. Rep. Online*, 2009, **65**, m455.
- 78 C. A. Kilner and M. A. Halcrow, An unusual discontinuity in the thermal spin transition in $[\text{Co}(\text{terpy})_2][\text{BF}_4]_2$, *Dalton Trans.*, 2010, **39**, 9008.
- 79 J. Palion-Gazda, A. Świtlicka-Olszewska, B. Machura, T. Granca, E. Pardo, F. Lloret and M. Julve, High-Temperature Spin Crossover in a Mononuclear Six-Coordinate Cobalt(II) Complex, *Inorg. Chem.*, 2014, **53**, 10009.
- 80 L. Váhovská, I. Potočná, S. Vitushkina, M. Dušek, J. Titiš and R. Boča, Low-dimensional compounds containing cyanido groups. XXVI. Crystal structure, spectroscopic and magnetic properties of Co(II) complexes with non-linear pseudohalide ligands, *Polyhedron*, 2014, **81**, 396.
- 81 X.-Y. Wang, L. Wang, Z.-M. Wang and S. Gao, Solvent-Tuned Azido-Bridged Co^{2+} Layers: Square, Honeycomb, and Kagomé, *J. Am. Chem. Soc.*, 2006, **128**(3), 674.
- 82 T.-F. Liu, D. Fu, S. Gao, Y.-Z. Zhang, H.-L. Sun, G. Su and Y.-J. Liu, An Azide-Bridged Homospin Single-Chain Magnet: $[\text{Co}(2,2'\text{-bithiazoline})(\text{N}_3)_2]_n$, *J. Am. Chem. Soc.*, 2003, **125**, 13976.
- 83 S. Y. Zhang, B. W. Wang, N. Xu, W. Shi, S. Gao and P. Cheng, Ferromagnetic interactions in EO-azido-bridged binuclear transition metal(II) systems: Syntheses, crystal structures and magnetostructural correlations, *Sci. China: Chem.*, 2012, **55**, 942.
- 84 D. Valigura, C. Rajnák, J. Moncol, J. Titiš and R. Boča, A mononuclear Co(II) complex formed from pyridinedimethanol with manifold slow relaxation channels, *Dalton Trans.*, 2017, **46**, 10950.
- 85 A. Świtlicka, B. Machura, M. Penkala, A. Bieńko, D. C. Bieńko, J. Titiš, C. Rajnák, R. Boča, A. Ozarowski and M. Ozerov, Slow Magnetic Relaxation in Cobalt(II) Field-Induced Single-Ion Magnets with Positive Large Anisotropy, *Inorg. Chem.*, 2018, **57**, 12740.
- 86 A. Bencini and D. Gatteschi, *In EPR of Exchange Coupled Systems*, Springer Verlag, Berlin/Heidelberg, 1990.
- 87 F. Neese, The ORCA program system, *Wiley Interdiscip. Rev. Comput. Mol. Sci.*, 2012, **2**, 73.
- 88 F. Neese, *ORCA – An Ab Initio, Density Functional and Semiempirical Program Package, Version 4.0.0*.
- 89 M. Atanasov, D. Ganyushin, D. A. Pantazis, K. Sivalingam and F. Neese, Detailed Ab Initio First-Principles Study of the Magnetic Anisotropy in a Family of Trigonal Pyramidal Iron(II) Pyrrolide Complexes, *Inorg. Chem.*, 2011, **50**, 7460.
- 90 C. Angeli, S. Borini, M. Cestari and R. Cimiraglia, A quasi-degenerate formulation of the second order n -electron valence state perturbation theory approach, *J. Chem. Phys.*, 2004, **121**, 4043.
- 91 C. Angeli, R. Cimiraglia, S. Evangelisti, T. Leininger and J. P. Malrieu, Introduction of n -electron valence states for multireference perturbation theory, *J. Chem. Phys.*, 2001, **114**, 10252.
- 92 C. Angeli, R. Cimiraglia and J. P. Malrieu, n -electron valence state perturbation theory: A spinless formulation and an efficient implementation of the strongly contracted and of the partially contracted variants, *J. Chem. Phys.*, 2002, **117**, 9138.
- 93 F. Neese, Efficient and accurate approximations to the molecular spin-orbit coupling operator and their use in molecular gg-tensor calculations, *J. Chem. Phys.*, 2005, **122**, 34107.
- 94 D. Ganyushin and F. Neese, First-principles calculations of zero-field splitting parameters, *J. Chem. Phys.*, 2006, **125**, 24103.
- 95 F. Neese, Calculation of the zero-field splitting tensor on the basis of hybrid density functional and Hartree-Fock theory, *J. Chem. Phys.*, 2007, **127**, 164112.
- 96 K. Yamaguchi, Y. Takahara and T. Fueno, in *Applied Quantum Chemistry*, ed. V. H. Smith, Reidel, Dordrecht, 1986, pp. 155.

- 97 F. Neese, Prediction of molecular properties and molecular spectroscopy with density functional theory: From fundamental theory to exchange-coupling, *Coord. Chem. Rev.*, 2009, **253**, 526.
- 98 C. Rajnák, A. Packová, J. Titiš, J. Miklovič, J. Moncol and R. Boča, A tetracoordinate Co(II) single molecule magnet based on triphenylphosphine and isothiocyanato group, *Polyhedron*, 2016, **110**, 85.
- 99 L. Smolko, J. Černák, M. Dušek, J. Miklovič, J. Titiš and R. Boča, Three tetracoordinate Co(II) complexes [Co(biq)X₂] (X=Cl, Br, I) with easy-plane magnetic anisotropy as field-induced single-molecule magnets, *Dalton Trans.*, 2015, **44**, 17565.
- 100 A. Packová, J. Miklovič and R. Boča, Manifold relaxation processes in a mononuclear Co(II) single-molecule magnet, *Polyhedron*, 2015, **102**, 88.
- 101 R. Boča, J. Miklovič and J. Titiš, Simple Mononuclear Cobalt(II) Complex: A Single-Molecule Magnet Showing Two Slow Relaxation Processes, *Inorg. Chem.*, 2014, **53**, 2367.
- 102 C. Rajnák, J. Titiš, O. Fuhr, M. Ruben and R. Boča, Single-Molecule Magnetism in a Pentacoordinate Cobalt(II) Complex Supported by an Antenna Ligand, *Inorg. Chem.*, 2014, **53**, 8200.
- 103 M. Atzori, L. Tesi, E. Morra, M. Chiesa, L. Sorace and R. Sessoli, Room-Temperature Quantum Coherence and Rabi Oscillations in Vanadyl Phthalocyanine: Toward Multifunctional Molecular Spin Qubits, *J. Am. Chem. Soc.*, 2016, **138**, 2154.
- 104 M. Ding, G. E. Cutsail, D. Aravena, M. Amoza, M. Rouzières, P. Dechambenoit, Y. Losovyj, M. Pink, E. Ruiz, R. Clérac and J. M. Smith, A low spin manganese(IV) nitride single molecule magnet, *Chem. Sci.*, 2016, **7**, 6132.
- 105 R. Boča, C. Rajnák, J. Titiš and D. Valigura, Field Supported Slow Magnetic Relaxation in a Mononuclear Cu(II) Complex, *Inorg. Chem.*, 2017, **56**, 1478.
- 106 A. Świtlicka, B. Machura, R. Kruszynski, J. Cano, L. M. Toma, F. Lloret and M. Julve, The influence of pseudohalide ligands on the SIM behaviour of four-coordinate benzylimidazole-containing cobalt(II) complexes, *Dalton Trans.*, 2018, **47**, 5831.
- 107 R. Herchel, L. Váhovská, I. Potočňák and Z. Trávníček, Slow magnetic relaxation in octahedral cobalt(II) field-induced single-ion magnet with positive axial and large rhombic anisotropy, *Inorg. Chem.*, 2014, **53**, 5896.
- 108 C. Rajnák, J. Titiš, J. Moncol, F. Renz and R. Boča, Field supported slow magnetic relaxation in hexacoordinate Co(II) complexes with easy plane anisotropy, *Eur. J. Inorg. Chem.*, 2017, 1520.
- 109 E. A. Buvaylo, V. N. Kokozay, O. Y. Vassilyeva, B. W. Skelton, A. Ozarowski, J. Titiš, B. Vranovičová and R. Boča, Field-Assisted Slow Magnetic Relaxation in a Six-Coordinate Co(II)-Co(III) Complex with Large Negative Anisotropy, *Inorg. Chem.*, 2017, **56**, 6999.
- 110 E. Ruiz, J. Cirera, J. Cano, S. Alvarez, C. Loose and J. Kortus, Can large magnetic anisotropy and high spin really coexist?, *Chem. Commun.*, 2008, 52.